Extension of the acousto-optic Bragg regime through Hamming apodization of the sound field

R. Pieper* and A. Korpel

Department of Electrical and Computer Engineering, University of Iowa, Iowa City, Iowa 52242

W. Hereman†

Instituut voor Theoretische Mechanica, Rijksuniversiteit Gent, B-9000 Gent, Belgium

Received September 12, 1985; accepted April 24, 1986

It is argued from a physical point of view that the criteria for acousto-optic Bragg diffraction (characterized by only two orders of light being present) must ultimately include the strength of the sound field. This follows because the scattering effect that is due to the sidelobes of a rectangular transducer, although negligible at low power levels where the Bragg criterion is indeed sound-level independent, becomes of increasing importance at high power levels and causes additional orders to be generated. In this paper we demonstrate this numerically by reduction of the sidelobes through Hamming apodization of the sound field. The results clearly demonstrate a significant reduction in the light powers of the spurious orders, thereby extending Bragg operation to higher sound intensities than normally feasible.

INTRODUCTION

Since the observations of Debye and Sears,[1] there has been interest in developing reliable criteria for determining the conditions in which only one order is significantly diffracted. References 2–5 present an incomplete list of various workers who have proposed criteria marking the threshold of the Bragg regime. The fact that these criteria were primarily motivated in one case by physical considerations[2,3] and in the other case by mathematical considerations[4,5] has led to some confusion in the literature, especially regarding the role played by the sound level. The work presented here lends some insight into this problem by heuristic arguments and numerical simulations that dramatically illustrate the effect of acoustic sidelobes on Bragg-type behavior for high sound levels. A detailed comparison of the various criteria in light of this investigation is now in preparation.

A BRIEF REVIEW OF ACOUSTO-OPTIC PRINCIPLES

To keep this paper self-contained, we briefly review the principles of acousto-optics. Table 1 lists the various fundamental parameters appearing in this discussion. The uppercase symbols have generally been reserved for acoustic parameters. The following standard wave relationships exist between wave numbers K, k and wavelengths Λ, λ and radian frequencies Ω, ω:

$$K = \frac{2\pi}{\Lambda} = \frac{\Omega}{V_s}, \tag{1a}$$

$$k = \frac{2\pi}{\lambda} = \frac{\omega}{c}. \tag{1b}$$

The Bragg angle ϕ_B, defining a condition for acousto-optic interaction,[6] is easily obtained from the conservation of momentum diagram shown in Fig. 1. From this diagram it follows that the Bragg angle satisfies the expression

$$\sin \phi_B = \frac{1}{2}\frac{K}{k}.$$

In the practical acousto-optic regime of interest, the acoustic wave speed and frequency are much less than their optical counterparts. Consistent with the assumption $K \ll k$, the Bragg angle ϕ_B is then given approximately by

$$\phi_B \simeq \frac{1}{2}\frac{K}{k}. \tag{2}$$

The momentum triangle as shown in Fig. 1 is nearly isosceles since the difference between the incident and diffracted optical wave numbers is negligible.[6]

The momentum triangle can be satisfied in two physically distinct ways,[6] depending on the incident angle ϕ_o (measured counterclockwise positive). First, in the case of phonon absorption [Fig. 2(a)], the angle χ_+ between the directions of incident light and sound propagation satisfies

$$\chi_+ = 90° - \phi_B, \tag{3}$$

where $\phi_0 = -\phi_B$.

In the case of stimulated phonon emission [Fig. 2(b)], the angle χ_- satisfies

$$\chi_- = 90° + \phi_B, \tag{4}$$

where $\phi_0 = +\phi_B$.

Because phonon absorption and emission also satisfy energy conservation, these processes lead to frequency upshifting and downshifting, respectively, in the diffracted photon as dictated by Eqs. (5a) and (5b):

$$\omega^+ = \omega + \Omega, \tag{5a}$$

$$\omega^- = \omega - \Omega. \tag{5b}$$

0740-3232/86/101608-12$02.00

Table 1. Fundamental Parameters

Description	Acoustic	Optical	
Wavelength	Λ	$\gg$	λ
Wave speed	V_s	$\ll$	c
Radian frequency	Ω	$\ll$	ω
Wave number	K	$\ll$	k

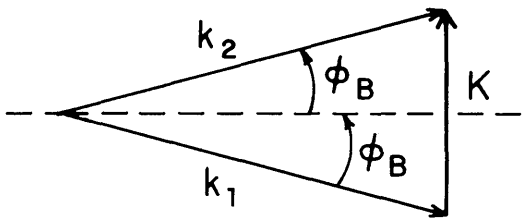

Fig. 1. Momentum diagram for acousto-optic Bragg scattering.

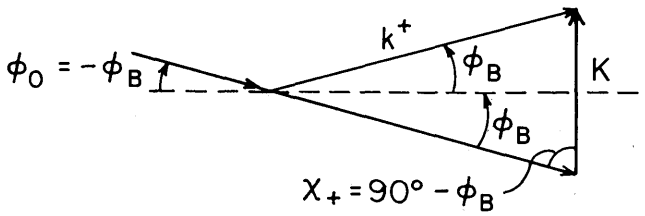

(a)

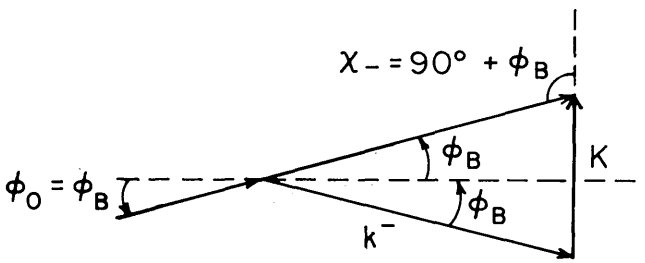

(b)

Fig. 2. Bragg momentum diagrams corresponding to (a) photo-emission and (b) absorption.

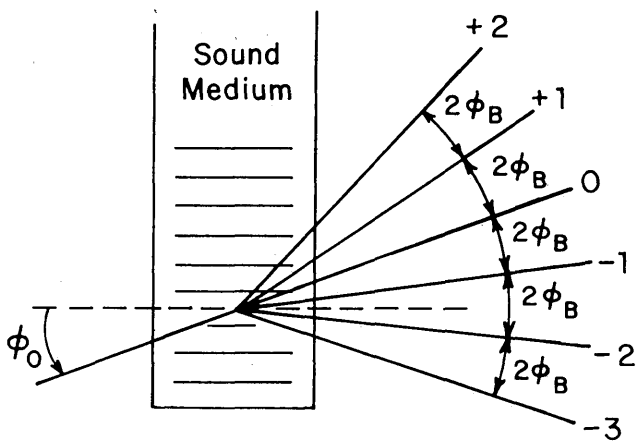

Fig. 3. Various diffracted orders of light that result from multiple scattering.

Hence the phonon-emission process generates from the incident zeroth order a photon in the frequency downshifted minus-one order, while conversely the absorption process leads to the frequency upshifted plus-one order.

In general it is possible to have multiple scattering of light, such as $0 \rightarrow +1 \rightarrow +2$. As represented in Fig. 3, adjacent orders of light will be separated by $2\phi_B$, in agreement with Fig. 1. The nth-order normalized light intensities, I_n, can be obtained from the nth-order electric field amplitudes E_n by using

$$I_n = E_n E_n^*, \tag{6}$$

where the asterisk denotes the complex conjugate.

The multiple-scattering process is dependent on the angular plane-wave spectrum of sound $\tilde{S}(\gamma)$, where γ, the angle measured relative to the nominal direction of the sound beam, is defined by Fig. 4. Following standard transform techniques,[7] the angular sound spectrum can be obtained from the sound field $S(z)$ by the relations

$$\tilde{S}(\gamma) = F[S(z)]|_{w=\gamma/\Lambda}, \tag{7}$$

where

$$F[S(z)] = \int_{-\infty}^{\infty} S(z)\exp(-j2\pi wz)\mathrm{d}z,$$

and the sound field $S(z)$ satisfies the standard engineering phasor convention for waves propagating in the $+X$ direction, i.e.,

$$S(z, x, t) = \mathrm{Re}[S(z)\exp(j\Omega t - jKx)]. \tag{8}$$

HEURISTIC BRAGG REGIME ANALYSIS VALID FOR MOST ACOUSTO-OPTIC APPLICATIONS

For a uniform sound field of width L the angular plane-wave power spectrum can be shown readily to have the form

$$P(\bar{\gamma}) = \mathrm{sinc}^2(\bar{\gamma}), \tag{9}$$

where a normalized angle $\bar{\gamma}$ is defined by

$$\bar{\gamma} = \frac{\gamma L}{\Lambda} \tag{10}$$

and

$$\mathrm{sinc}(X) = \frac{\sin(\pi X)}{\pi X}. \tag{11}$$

The decibel power spectrum of Eq. (9), plotted as the solid curve in Fig. 5, is given by

$$\mathrm{dB}\, P(\bar{\gamma}) = 10 \log[P(\bar{\gamma})]. \tag{12}$$

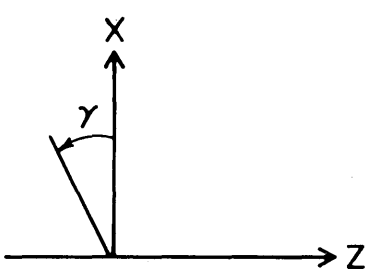

Fig. 4. Convention for positive angle used in angular plane-wave spectrum.

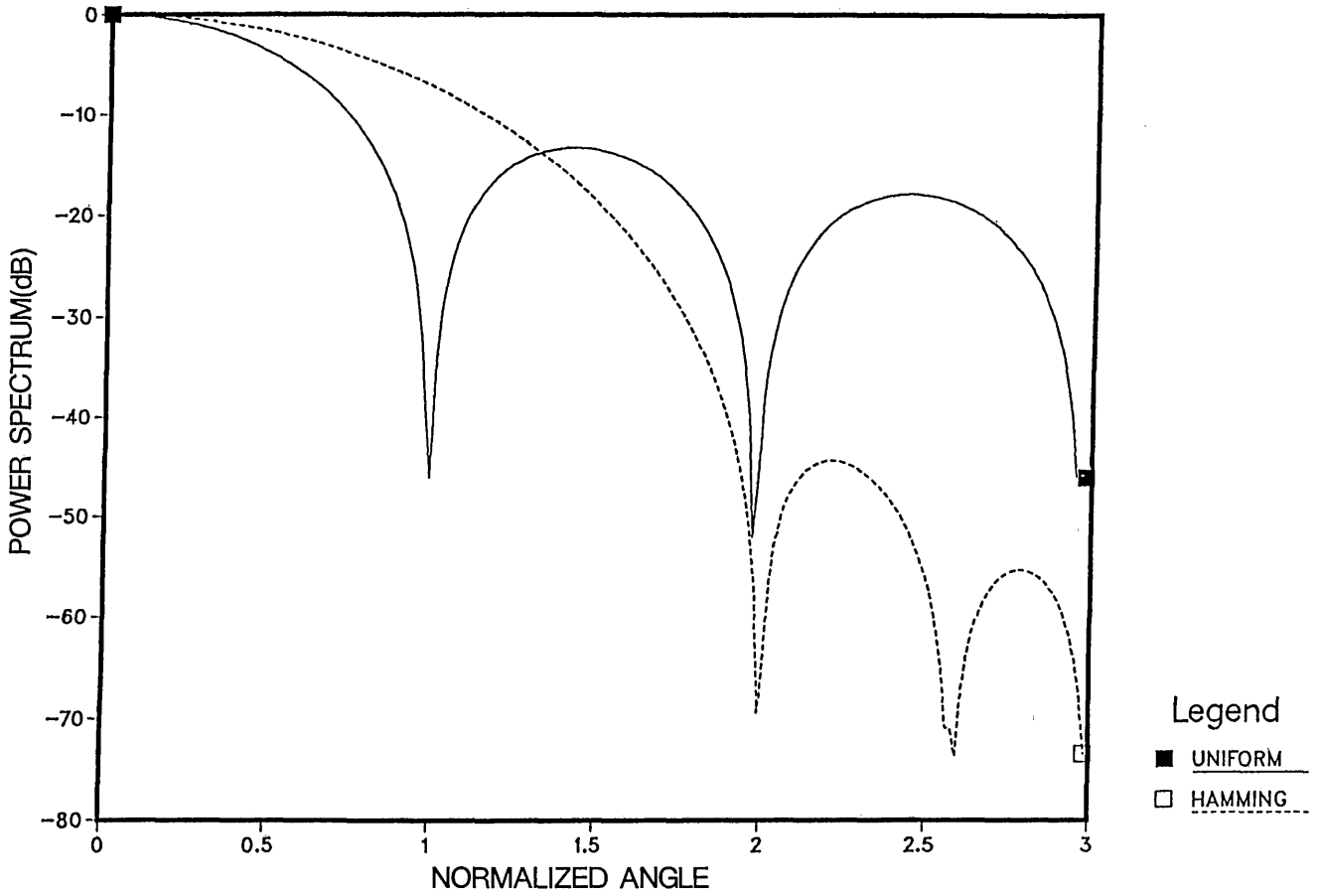

Fig. 5. The decibel power spectrum for uniform and Hamming-apodized fields.

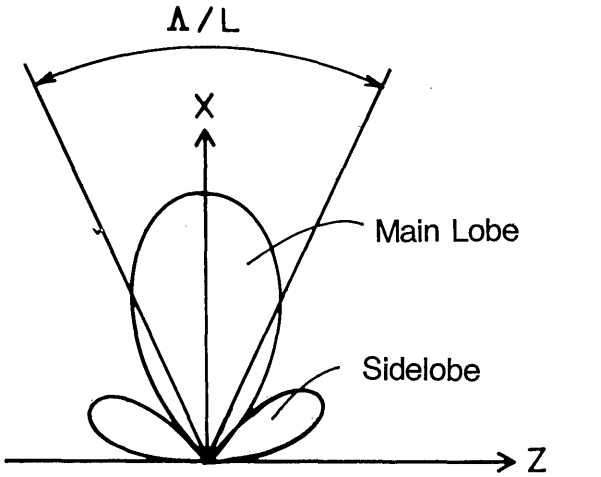

Fig. 6. A measure for the width of the main lobe of the uniform sound field.

As indicated on the radiation diagram of Fig. 6, a measure for the width of the main lobe is Λ/L being the location of the first zero. According to Eq. (12), at half this value, i.e., at $|\bar{\gamma}| = 1/2$, the power spectrum has decreased by 3.9 dB (roughly 40%). Assuming that the part of the sound spectrum power predominantly responsible for multiple scattering of light lies within the main lobe, we can readily derive the usual criterion for the Bragg regime (i.e., the regime in which only one order is significantly diffracted). In order to avoid, from within the main lobe, the simultaneous generation of both the plus-one and the minus-one orders, it is clear from Eqs. (3) and (4) and the (most pessimistic, i.e., normally incident) limiting case shown in Fig. 7 that the following condition must be satisfied:

$$2\frac{\Lambda}{L} < 2\phi_B. \tag{13}$$

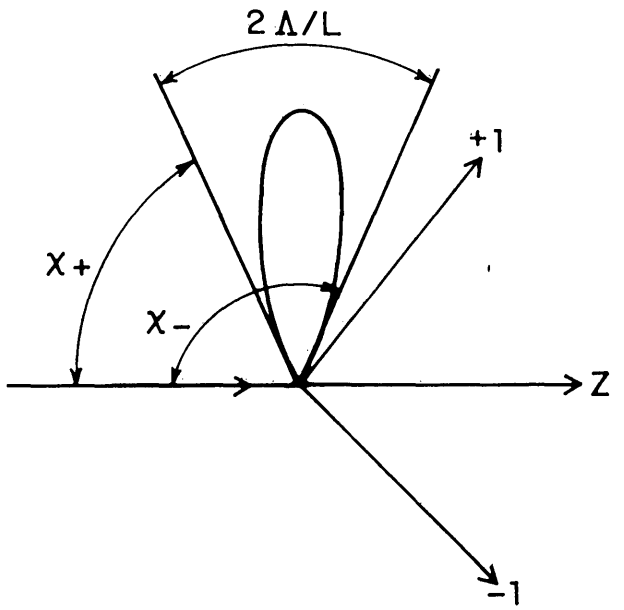

Fig. 7. Main lobe of sound field at the threshold for simultaneous generation of both the +1 and the −1 orders.

It follows from expression (2) that an equivalent form for this condition is

$$L > 2\Lambda^2/\lambda. \tag{14}$$

In terms of the Klein–Cook coefficient,[3] $Q = LK^2/k$, expression (13) leads to the condition $Q > 4\pi$.

One of the critical assumptions in the above simplistic analysis is that the acoustic power in the sidelobes can be neglected in the diffraction process. This assumption is valid for sound-intensity levels necessary for most applications to date, and expression (14) is adequate for defining the Bragg region. For arbitrarily high sound intensities, however, this assumption is not justified, and expression (14) does not adequately define the Bragg regime.

FORMALISM FOR STRONG ACOUSTO-OPTIC INTERACTION BETWEEN PLANE WAVES OF LIGHT AND SOUND

From Ref. 8 we state the generally valid coupled equations for the plane-wave amplitudes of scattered light $E_n(z)$:

$$\frac{dE_n}{dz} = -j(a_{n-1}S_{n-1}^{+}(z)E_{n-1} + a_{n+1}S_{n+1}^{-}(z)E_{n+1}), \tag{15}$$

where, in agreement with Fig. 3, the nth-order light term propagates along the specific directions:

$$\phi_n = \phi_0 + 2n\phi_B, \tag{16}$$

appearing on Fig. 8 as solid lines. The order-coupling coefficients $S_n^{+}(z)$ and $S_n^{-}(z)$ are evaluated according to

$$S_n^{+}(z) = S[z, z\tan(\phi_n + \phi_B)], \tag{17}$$

$$S_n^{-}(z) = S^*[z, z\tan(\phi_n - \phi_B)], \tag{18}$$

where it follows from Eq. (8) that

$$S(z, x) = S(z)\exp(-jKx). \tag{19}$$

Referring to Fig. 8, Eqs. (17) and (18) correspond to evaluating the sound field $S(z, x)$ along so-called Bragg lines, which are shown as the dashed bisectors of the solid lines. Finally, the acousto-optic interaction coefficient a_n is given by

$$a_n = -kn^2p/(4\cos\phi_n) \qquad \text{for } n = 0, \pm1, \pm2, \pm3, \ldots, \tag{20}$$

where n is the index of refraction and p is the strain optic coefficient. Owing to the assumption of small Bragg angles and nearly normal incidence, valid in most practical cases, $\cos\phi_n \simeq +1$ and, therefore,

$$a_n \simeq -kn^2p/4 \equiv a, \qquad n = 0, \pm1, \pm2, \pm3, \ldots, \tag{21}$$

where $a_n = a$ is dependent only on material parameters. Consistent with the assumption of small diffraction angles, Eqs. (17) and (18) become

$$S_n^{+} \simeq S[z, z(\phi_n + \phi_B)], \tag{22}$$

$$S_n^{-} \simeq S^*[z, z(\phi_n - \phi_B)]. \tag{23}$$

It follows from Eqs. (16) and (19) and expressions (22) and (23) that

$$S_{n-1}^{+}(z) = S(z)\exp\{-jKz[\phi_0 + (2n-1)\phi_B]\}, \tag{24}$$

$$S_{n+1}^{-}(z) = S^*(z)\exp\{+jKz[\phi_0 + (2n+1)\phi_B]\}. \tag{25}$$

Without loss of generality, we take $z = 0$ to correspond to the left edge of the sound field of finite length L.

Following the normalization procedure of Ref. 9, Eqs. (15), (21), (24), and (25) can be posed in a normalized form, thereby obviating specification of actual sound frequencies and design lengths. This process is implemented through the normalized parameters presented in Table 2. In terms of the variables of this table, Eqs. (24) and (25) become

$$S_{n-1}^{+}(\bar{z}) = S(\bar{z})\exp\left[-jQ_c\bar{\Omega}^2\bar{z}\left(\frac{\bar{\phi}_0}{\bar{\Omega}} + 2n - 1\right)\Big/2\right], \tag{26}$$

$$S_{n+1}^{-}(\bar{z}) = S^*(\bar{z})\exp\left[+jQ_c\bar{\Omega}^2\bar{z}\left(\frac{\bar{\phi}_0}{\bar{\Omega}} + 2n + 1\right)\Big/2\right], \tag{27}$$

and Eq. (15) becomes

$$\frac{dE_n}{d\bar{z}} = -jaL[S_{n-1}^{+}(\bar{z})E_{n-1} + S_{n+1}^{-}(\bar{z})E_{n+1}], \tag{28}$$

with the initial conditions

$$\begin{aligned} &E_n(\bar{z} = 0) = 0, \qquad n = \pm1, \pm2, \pm3, \ldots, \\ &E_0(\bar{z} = 0) = 1.0. \end{aligned} \tag{29}$$

Once $S(z)$ is defined, the order-coupling coefficients S_{n-1}^{+} and S_{n+1}^{-} are determined through Eqs. (26) and (27). Equation (28) can be numerically space integrated to yield the complex field amplitudes $E_n(\bar{z} = 1)$. The output light intensities I_n are obtained through the relation

$$I_n = E_n(\bar{z} = 1)E_n^*(\bar{z} = 1). \tag{30}$$

We make the convenient choices as shown below for the normalized frequency $\bar{\Omega}$ and incident angle $\bar{\phi}_0$:

$$\bar{\Omega} = 1.0, \tag{31a}$$

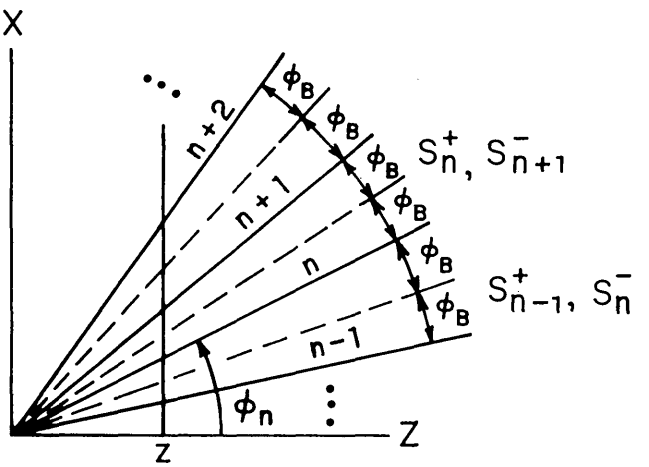

Fig. 8. General interaction diagram showing (dashed) Bragg lines.

Table 2. Normalized Parameters[a]

z coordinate	$\bar{z} = z/L$
Frequency	$\bar{\Omega} = \Omega/\Omega_c$
Incident angle	$\bar{\phi}_0 = \phi_0/\phi_{B_c}$
Klein–Cook parameter	$Q_c = L(K_c^2/k)$
Angular spectrum variable	$\bar{\gamma} = \gamma L/\Lambda$

[a] Subscript c indicates evaluation at the center frequency.

$$\bar{\phi}_0 = 1.0, \tag{31b}$$

leaving only the Klein–Cook parameter Q_c, which is indicative of the sound-field length, to be defined in Eqs. (26) and (27).

THE UNIFORM SOUND FIELD

The idealized (nonspreading) uniform sound field takes the usual form:

$$S_u(\bar{z}) = |S| W_u(\bar{z}), \quad \text{where } W_u(\bar{z}) = 1 \quad 0 \leqslant \bar{z} \leqslant 1, \quad = 0 \quad \text{otherwise.} \tag{32}$$

An amplitude factor

$$\beta = \frac{a|S|L}{\pi/2} \tag{33}$$

is defined in such a way that for exact Bragg incidence, i.e., $\phi_0 = \phi_B$, a value $\beta = 1.0$ leads to a maximum in energy transfer to the minus-one order.[6]

Once the Klein–Cook parameter Q_c is defined, Eq. (28) can be integrated numerically to obtain the light intensities $I_n(\bar{z} = 1)$, which can be plotted versus the sound amplitude factor β.

THE HAMMING-APODIZED SOUND FIELD

The Hamming window function[10] defined by

$$W_H(\bar{z}) = 0.54 + 0.46 \cos 2\pi(\bar{z} - 1/2) \quad 0 \leqslant \bar{z} \leqslant 1, \quad = 0 \quad \text{otherwise,} \tag{34}$$

is known to lead to significant reduction in sidelobe power when compared with the uniform field case. The power spectrum of Eqs. (34) is derived in Appendix A and, for comparison with Eq. (12), is plotted as the dashed curve shown in Fig. 5.

The idealized Hamming sound field can thus be written analogously to the uniform sound field:

$$S_H(\bar{z}) = |S| W_H(\bar{z}), \tag{35}$$

or in terms of β, by using Eq. 33,

$$S_H(\bar{z}) = \frac{\pi\beta}{2aL} W_H(\bar{z}).$$

NUMERICAL RESULTS

For the Klein–Cook parameters $Q_c = 3\pi$, 4π, 6π, and 8π, diffracted light-intensity plots for the uniform sound field [Eq. (32)] are shown in Figs. 9, 10, 11, and 12, respectively; for the Hamming sound field [Eq. (35)], the respective plots are Figs. 13, 14, 15, and 16. Although the numerical calculations employ ten orders, only two orders are plotted in the interest of clarity.

For the sake of completeness it is shown analytically in Appendix B that for ideal Bragg diffraction, when a uniform sound field is used, the intensity zeros for the minus-one order occur at amplitude factors

$$\beta_m = 2m, \qquad m = 0, 1, 2, \ldots, \tag{36}$$

while for the zeroth order the intensity zeros occur at

$$\beta_m = 2m + 1, \qquad m = 0, 1, 2, \ldots. \tag{37}$$

It is clear from examination of Figs. 9–12 that Bragg behavior breaks down at high sound amplitudes but that longer devices (higher Q_c) exhibit Bragg behavior over a wider range. It is interesting to note the total power in the spurious orders after one sound-amplitude cycle, i.e., $\beta = 2$:

30%	$Q_c = 3\pi$	(Fig. 9),
17%	$Q_c = 4\pi$	(Fig. 10),
10%	$Q_c = 6\pi$	(Fig. 11),
7%	$Q_c = 8\pi$	(Fig. 12).

(38)

In Appendix B it is shown analytically that for the assumption of Bragg diffraction (i.e., using two orders), when applying a Hamming-apodized sound field, the intensity zeros for the minus-one order occur at the amplitude factors

$$\beta_m = 3.7m, \qquad m = 0, 1, 2, \ldots, \tag{39}$$

while for the zeroth order the intensity zeros occur at

$$\beta_m = 3.7m + 1.85, \qquad m = 0, 1, 2, \ldots. \tag{40}$$

The actual numerical plots in Figs. 13–16 demonstrate a quasi-periodicity that agrees with Eqs. (39) and (40) in the high-Q low-sound-amplitude limit. At higher amplitudes, however, the period increases although complete power transfer still takes place. This would indicate that, although two orders appear only at the device output, a complete description requires more orders. Indeed, using the numerical formalism presented, it is possible to demonstrate that, although most of the *output* power is confined to the zero and minus-one orders, the other orders have a nontrivial interaction *within* the sound field, i.e., for $\bar{z} \leqslant 1$. As an illustration of this point we show, for the Hamming window configuration, two plots of light intensities [orders −1, 0 in Fig. 17(a); +1, −2 in Fig. 17(b)] versus the normalized coordinate $\bar{z}$, in which the sound-amplitude factor β is fixed at 10.0 and the Klein–Cook parameter Q_c is 8π. It is apparent from Fig. 17(a) that the total power in the sum of the intensities $(I_0 + I_{-1})$ is close to unity only at the exit $(\bar{z} = 1)$ of the sound field. Within the sound field the power loss in the two orders is for the most part accounted for by the diffraction of the light intensities I_{-2} and I_{+1}, as shown in Fig. 17(b). From these results we conclude that in order to verify *analytically* the quasi-periodicity that is evident in Figs. 13–16, at least the four orders I_0, I_{-1}, I_{-2}, and I_{+1} must be included.

In all cases ($Q_c = 3\pi$, 4π, 6π, and 8π) the Hamming-apodized sound field had less power transfer to external spurious orders than the uniform sound field. In particular, after one amplitude cycle, i.e., at $\beta = 3.7$, the power in the spurious orders for the Hamming window configuration turns out to be

3.0%	$Q_c = 3\pi$	(Fig. 13),
0.1%	$Q_c = 4\pi$	(Fig. 14),
<.1%	$Q_c = 6\pi$	(Fig. 15),
<.1%	$Q_c = 8\pi$	(Fig. 16).

(41)

Comparison of expressions (41) and expressions (38) also indicates that the Hamming-apodized sound field significantly restricts the power diffracted into spurious orders.

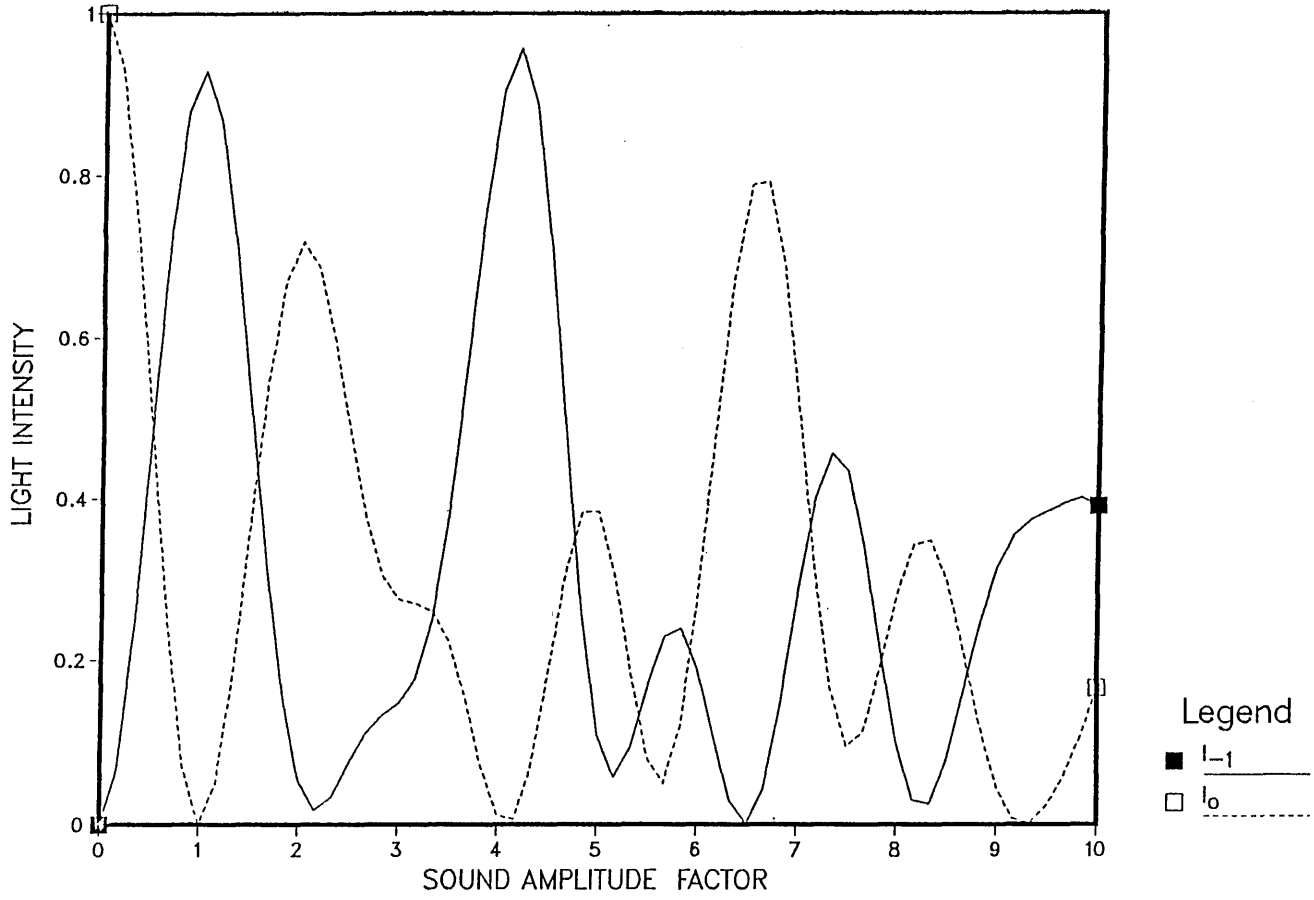

Fig. 9. Diffracted light intensities I_0 and I_{-1} versus the sound-amplitude factor for the uniform sound field with $Q_c = 3\pi$.

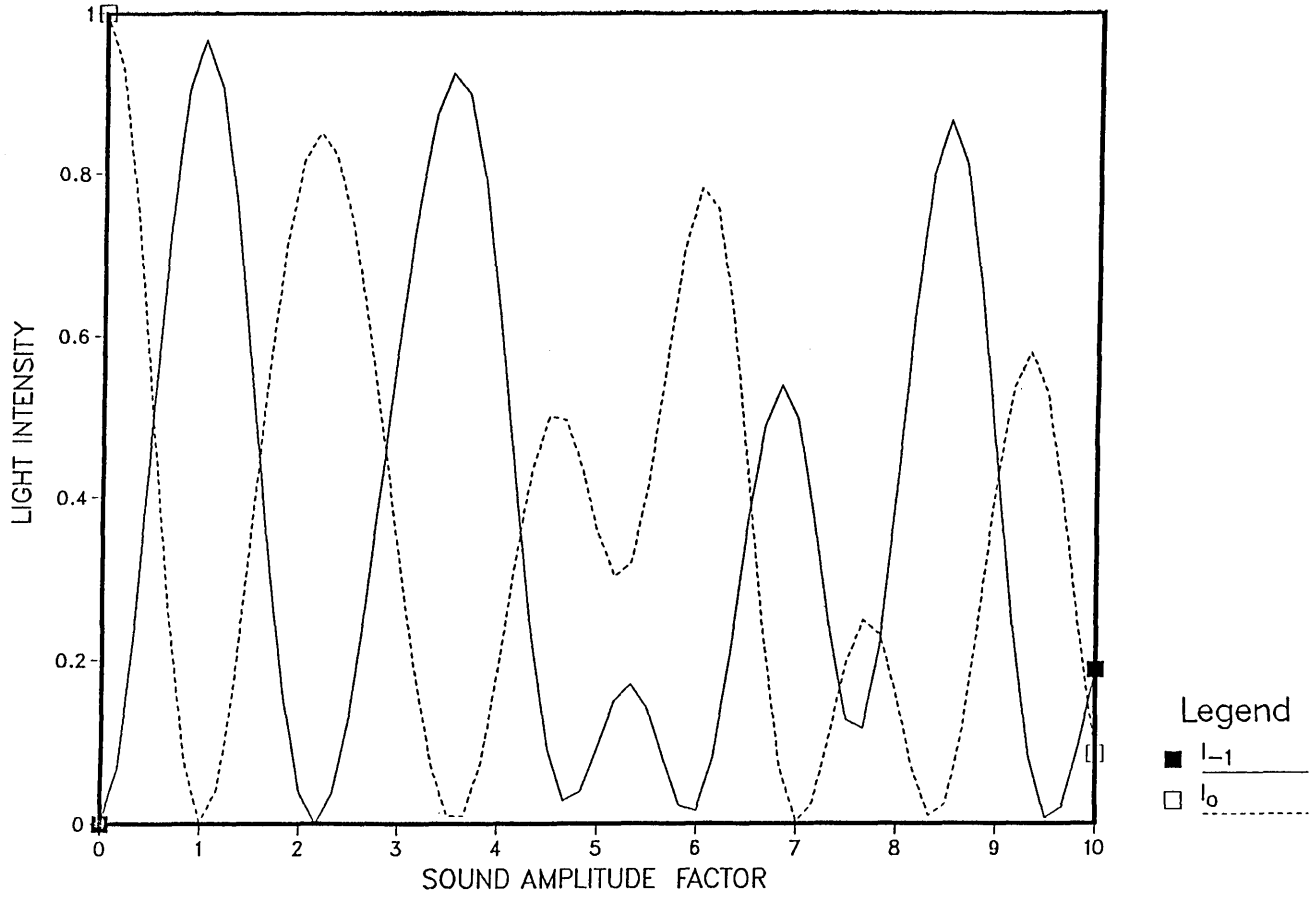

Fig. 10. Diffracted light intensities I_0 and I_{-1} versus the sound-amplitude factor for the uniform sound field with $Q_c = 4\pi$.

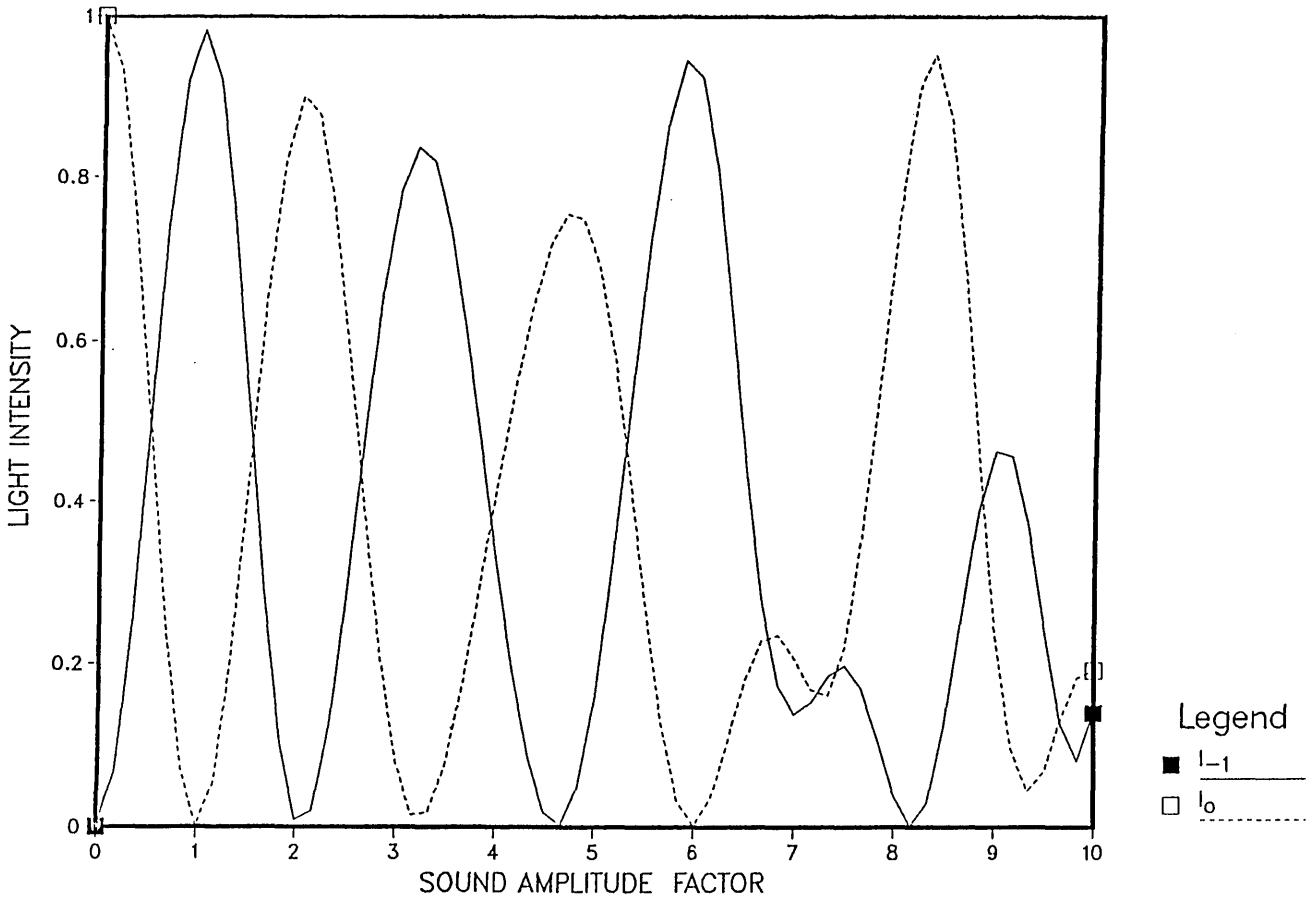

Fig. 11. Diffracted light intensities I_0 and I_{-1} versus the sound-amplitude factor for the uniform sound field with $Q_c = 6\pi$.

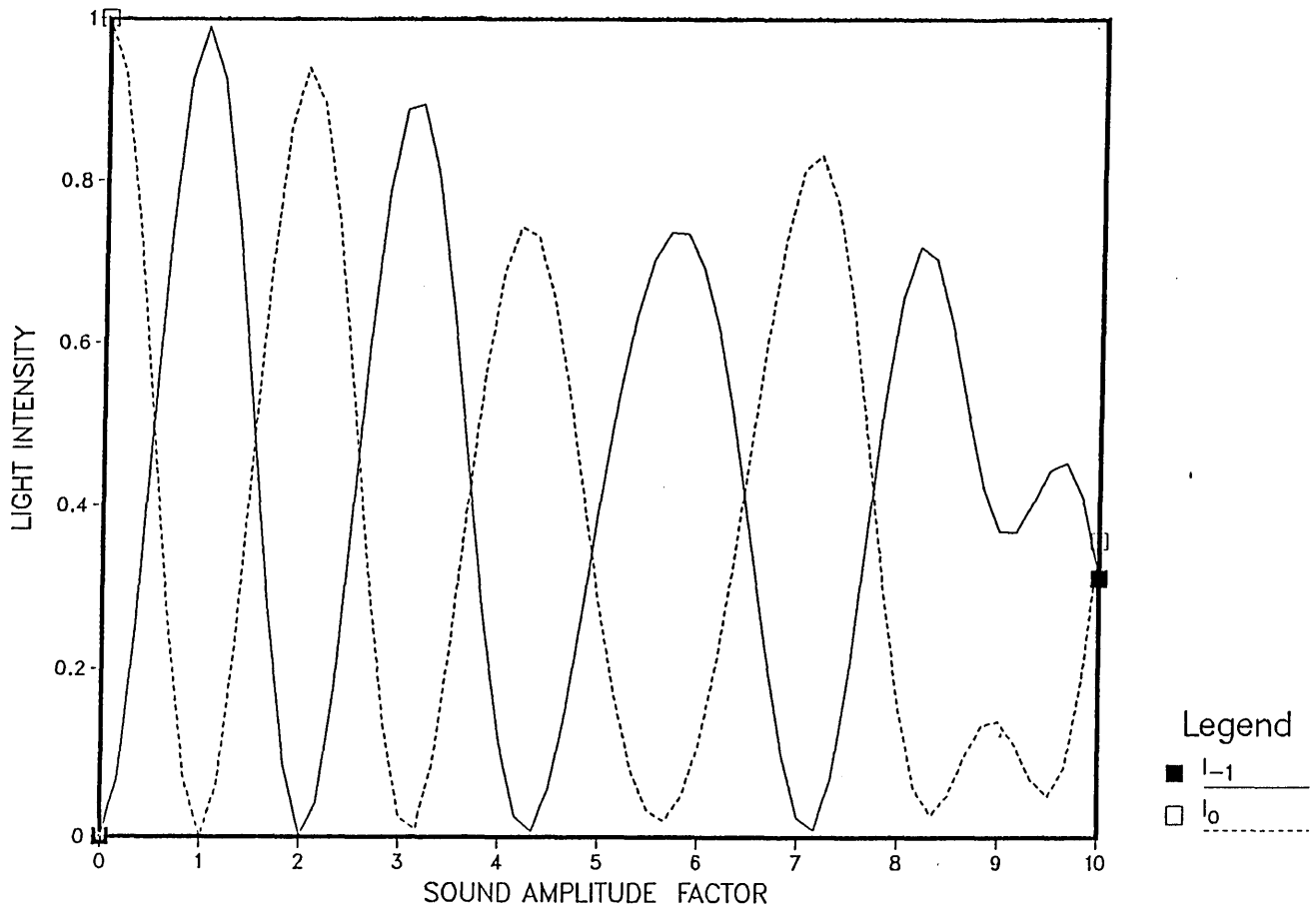

Fig. 12. Diffracted light intensities I_0 and I_{-1} versus the sound-amplitude factor for the uniform sound field with $Q_c = 8\pi$.

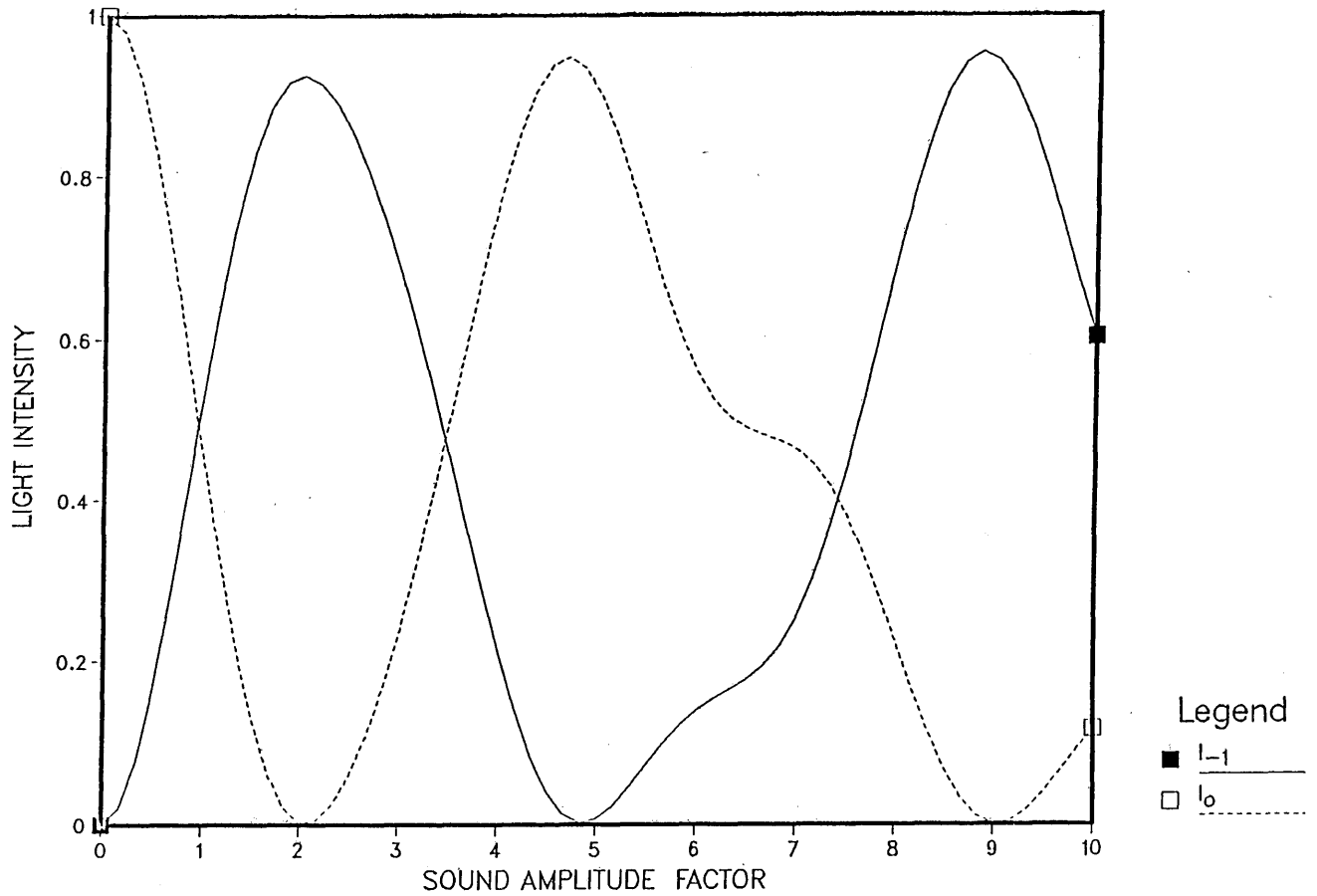

Fig. 13. Diffracted light intensities I_0 and I_{-1} versus the sound-amplitude factor for the Hamming-apodized sound field with $Q_c = 3\pi$.

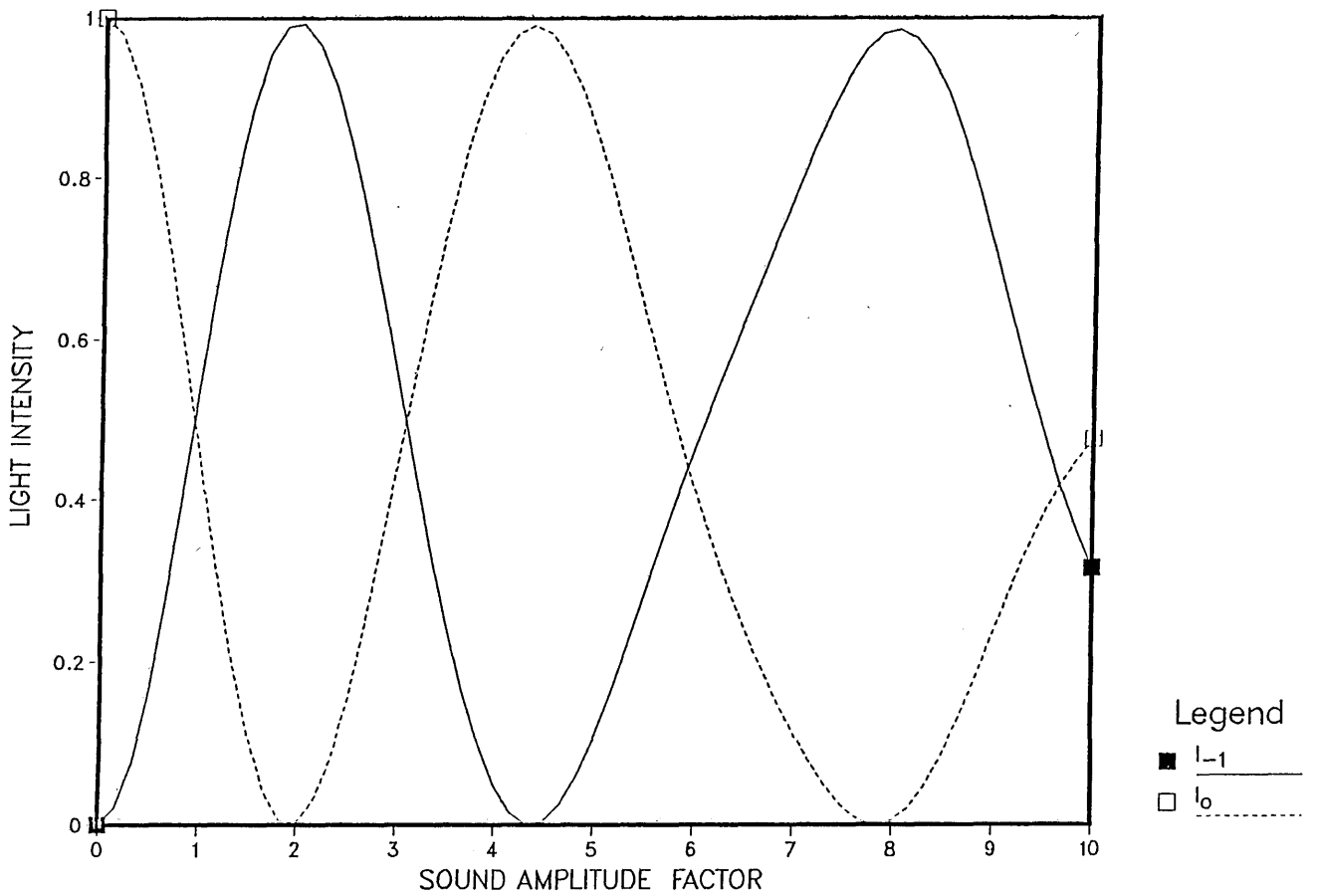

Fig. 14. Diffracted light intensities I_0 and I_{-1} versus the sound-amplitude factor for the Hamming-apodized sound field with $Q_c = 4\pi$.

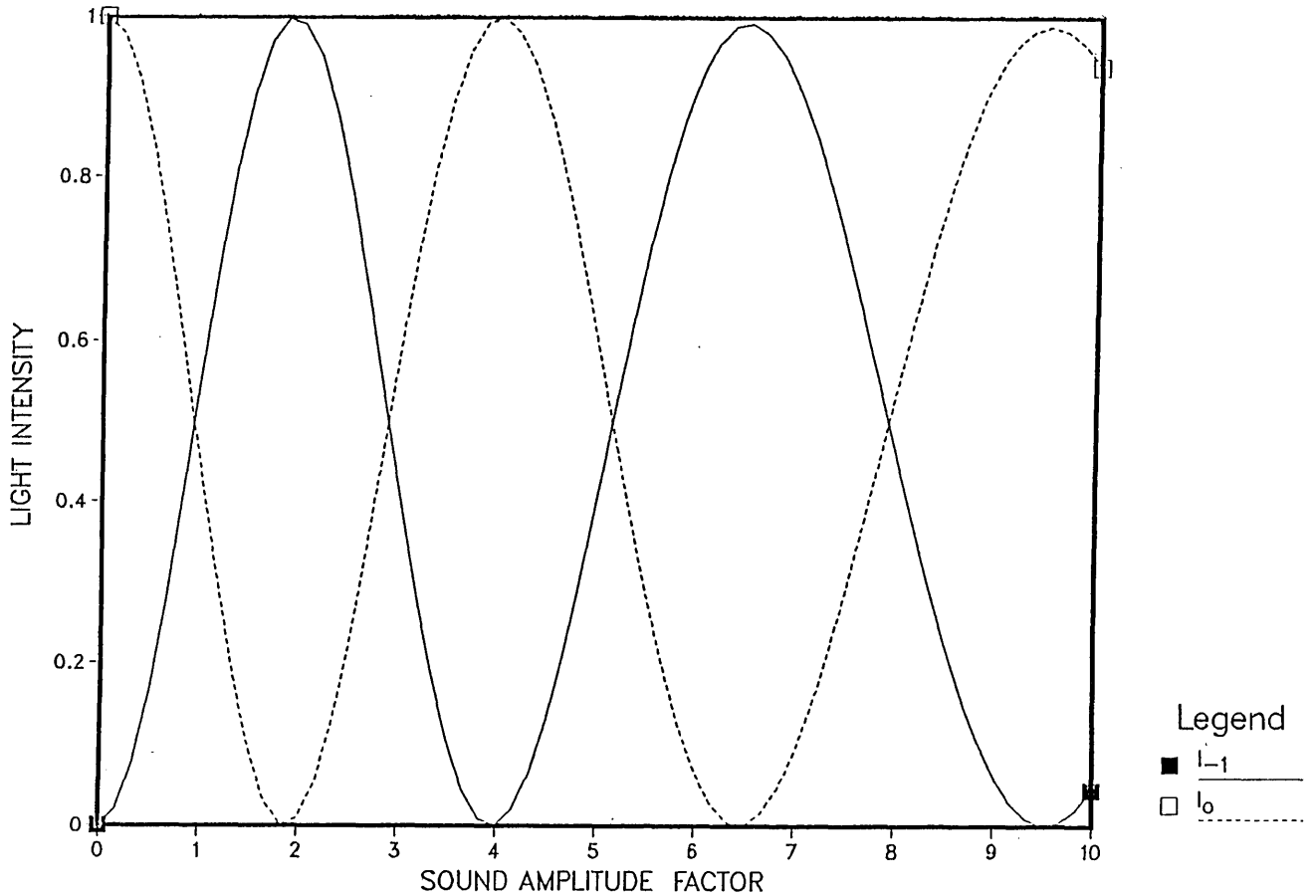

Fig. 15. Diffracted light intensities I_0 and I_{-1} versus the sound-amplitude factor for the Hamming-apodized sound field with $Q_c = 6\pi$.

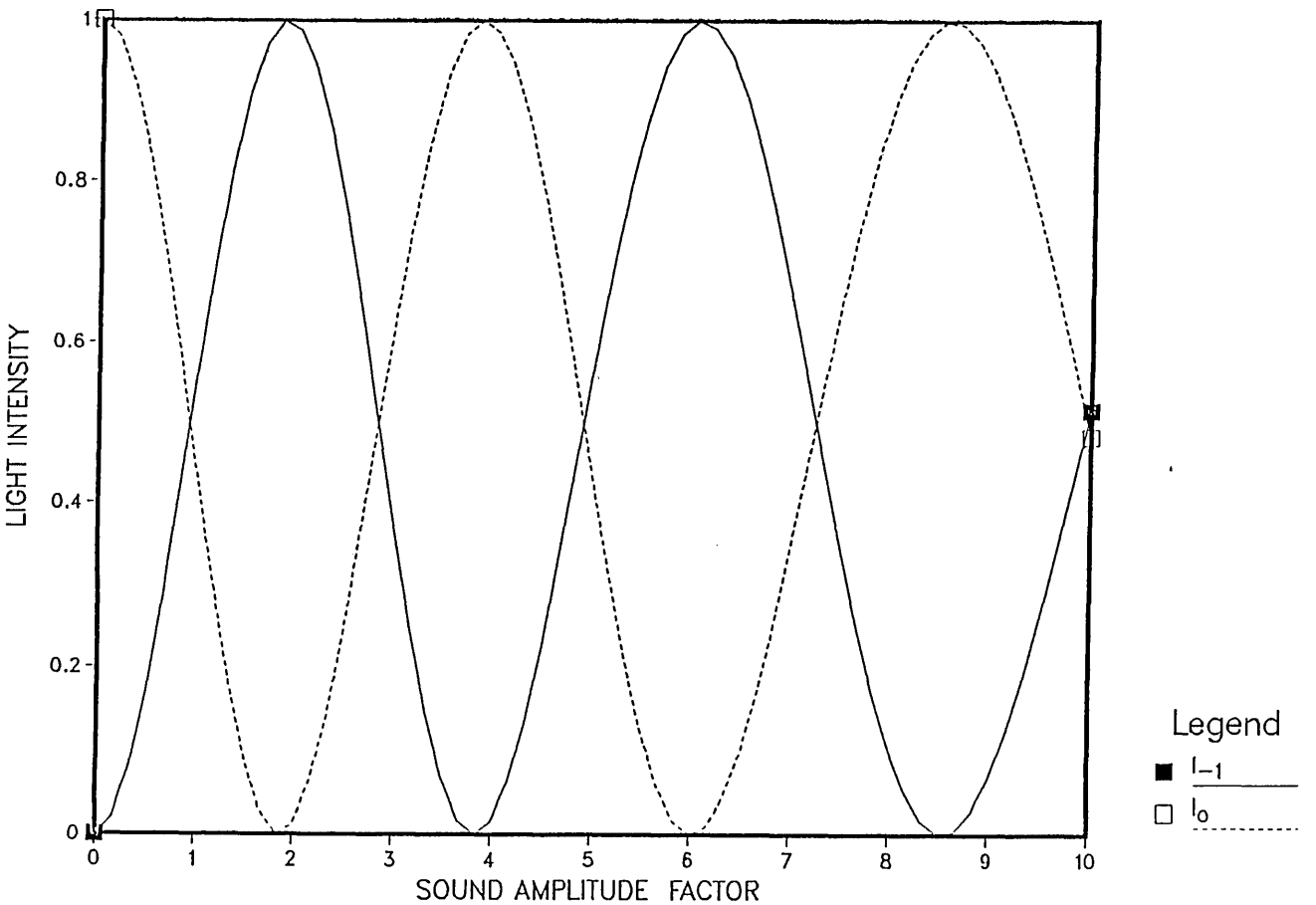

Fig. 16. Diffracted light intensities I_0 and I_{-1} versus the sound-amplitude factor for the Hamming-apodized sound field with $Q_c = 8\pi$.

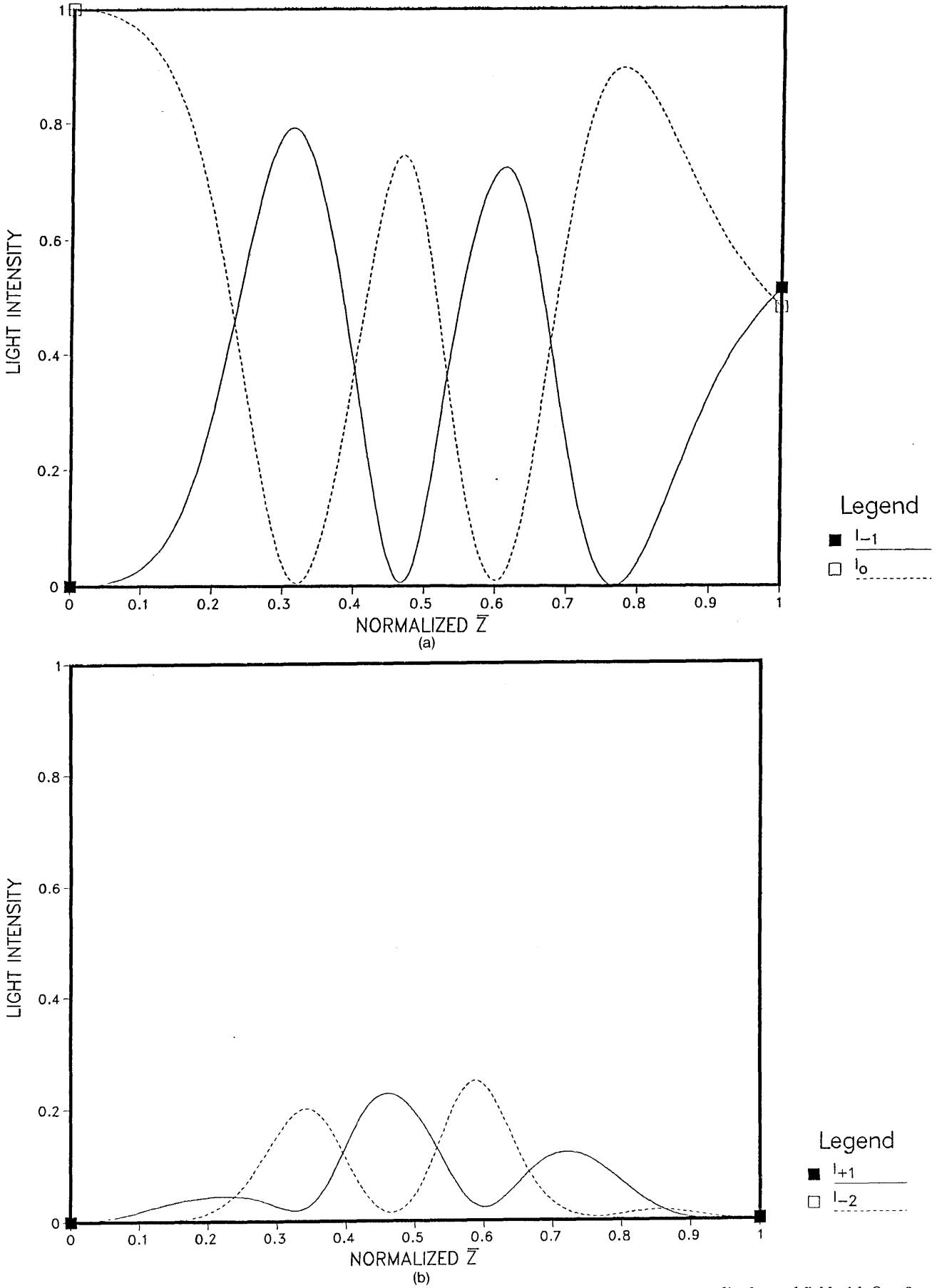

Fig. 17. (a) Diffracted light intensities I_0 and I_{-1} versus the normalized z coordinate for the Hamming-apodized sound field with $Q_c = 8\pi$ and $\beta = 10.0$. (b) Diffracted light intensities I_{+1} and I_{-2} versus the normalized z coordinate for the Hamming-apodized sound field with $Q_c = 8\pi$ and $\beta = 10.0$.

CONCLUSIONS

The numerical results confirm that acoustic sidelobes account for significant generation of spurious orders occurring at higher sound amplitudes, because after Hamming apodization of the sound field the generation of such spurious orders is significantly reduced. Evidently the Bragg regime is extended to higher sound amplitudes through reduction of these sidelobes. The presence of sidelobes thus appears to be the physical reason for the necessity of including sound-power considerations in the Bragg criteria.

A two-order analytic solution for the Hamming-apodized sound field agrees with the numerical results in the low-sound-amplitude limit. In general, however, the numerical solution demonstrates a quasi-periodicity that is conspicuously absent in the two-order analytic solution. This quasi-periodicity is shown to be connected with the existence of other orders inside the sound cell. The possibility of generating an analytic solution taking four orders into account is currently under investigation.

APPENDIX A

In this appendix we derive the angular plane-wave power spectrum associated with the Hamming-apodized sound field. For completeness we include the uniform sound field. The power spectrum is obtained from the squared magnitude of the angular plane-wave spectrum,[7] which can be normalized as shown:

$$P(\gamma) \equiv \frac{\tilde{S}(\gamma)\tilde{S}^*(\gamma)}{|\tilde{S}(0)|^2}. \tag{A1}$$

To avoid undue complexity in the analysis it is expedient to express sound fields [Eqs. (32) and (34)] in terms of a translated coordinate ζ, where

$$\zeta = z - L/2. \tag{A2}$$

In terms of ζ the sound fields [Eqs. (32) and (34)] become, respectively,

$$S_u(\zeta) = |S| \text{ rect}(\zeta/L) \tag{A3}$$

and

$$S_H(\zeta) = |S| \text{ rect}(\zeta/L)(0.54 + 0.46 \cos 2\pi\zeta/L), \tag{A4}$$

where

$$\begin{aligned} \text{rect}(\xi) &= 1 \quad \text{for } |\xi| < 0.5 \\ &= 0 \quad \text{for } |\xi| > 0.5. \end{aligned} \tag{A5}$$

Applying Eq. (7) and standard methods[7] to Eqs. (A3) and (A4), the angular plane-wave spectra are, respectively,

$$\tilde{S}_u(\bar{\gamma}) = \frac{|S|}{L} \text{sinc}(\bar{\gamma}) \tag{A6}$$

and

$$\tilde{S}_H(\bar{\gamma}) = 0.54 \frac{|S|}{L} \times \{\text{sinc}(\bar{\gamma}) + 0.426[\text{sinc}(\bar{\gamma} - 1/2) + \text{sinc}(\bar{\gamma} + 1/2)]\}, \tag{A7}$$

where the normalized angle $\bar{\gamma}$ has been defined by Eq. (10) in the text. Applying expression (A1) and Eq. (12), the decibel power spectra of Eqs. (A6) and (A7) are plotted versus $\bar{\gamma}$ in Fig. 5 as the solid and dashed curves, respectively.

APPENDIX B

In this appendix we derive analytical solutions for diffraction in the case that only two orders are considered for the sound fields, Eqs. (32) and (34).

Equation (15), when restricted to the two orders 0 and -1 and when subject to relation (21), reduces to

$$\frac{dE_0}{dz} = -jaS_{-1}{}^{+}E_{-1},$$

$$\frac{dE_{-1}}{dz} = -jaS_0{}^{-}E_0. \tag{B1}$$

In the case of a uniform sound field [Eq. (32)], it is easy to show from Eqs. (26) and (27) after employing condition (31) that

$$S_{-1}{}^{+} = S_0{}^{-*} = |S|. \tag{B2}$$

It follows after substitution of Eq. (B2) into Eqs. (B1) that the solution, subject to initial conditions [Eqs. (29)], can be written as

$$\begin{aligned} |E_0(z = L)|^2 &= \cos^2(a|S|L), \\ |E_{-1}(z = L)|^2 &= \sin^2(a|S|L). \end{aligned} \tag{B3}$$

Rewriting Eqs. (B3) in terms of the sound-amplitude factor [Eq. (33)] confirms the locations for the I_{-1} and I_0 intensity zeros at sound amplitudes [Eqs. (36) and (37)], respectively.

In the case of the Hamming-apodized sound field [Eq. (35)], it follows from Eqs. (26), (27), and (31) that

$$S_{-1}{}^{+} = S_0{}^{-*} = |S| W_H(z), \tag{B4}$$

where $W_H(z)$ is defined by Eqs. (34) after taking $\bar{z} = z/L$. Through the transformation

$$y(z) = 0.54z + \frac{0.46L}{2\pi} \sin\left[2\pi \frac{(z - L/2)}{L}\right], \tag{B5}$$

coupled equations (B1), subject to Eq. (B4), can be cast into the more tractable form

$$\frac{dE_0}{dy} = -ja|S|E_{-1},$$

$$\frac{dE_{-1}}{dy} = -ja|S|E_0. \tag{B6}$$

The solutions of Eqs. (B6), subject to initial conditions [Eq. (29)], can be written as

$$\begin{aligned} |E_0(z = L)|^2 &= \cos^2(0.54\, a|S|L), \\ |E_{-1}(z = L)|^2 &= \sin^2(0.54\, a|S|L). \end{aligned} \tag{B7}$$

Rewriting Eqs. (B7) in terms of the sound-amplitude factor [Eq. (33)] confirms the locations for the I_{-1} and I_0 intensity zeros [Eqs. (39) and (40)], respectively.

ACKNOWLEDGMENTS

R. Pieper and A. Korpel acknowledge the support of the National Science Foundation under grant ECS 8509942; W. Hereman would like to thank NATO for a Research Fellowship.

* Present address, Department of Electrical Engineering, Virginia Polytechnic and State University, Blacksburg, Virginia 24061.

† Present address, Department of Mathematics, University of Wisconsin–Madison, Madison, Wisconsin 53706.

REFERENCES

1. P. Debye and F. W. Sears, "On the scattering of light by supersonic waves," Proc. Natl. Acad. Sci. USA **18,** 409–414 (1932).
2. W. R. Klein and B. D. Cook, "Unified approach to ultrasonic light diffraction," IEEE Trans. Sonics Ultrason. **SU-14,** 123–133 (1967).
3. A. Korpel, "Acousto-optics—a review of fundamentals," Proc. IEEE **69,** 48–53 (1981).
4. T. K. Gaylord and M. G. Moharam, "Thin and thick gratings: terminology clarification," Appl. Opt. **20,** 3271–3273 (1981).
5. W. Hereman, R. Mertens, F. Verheest, O. Leroy, J. M. Claeys, and E. Blomme, "Interaction of light and ultrasound," Phys. Mag. **6,** 213–245 (1984).
6. A. Korpel, in *Applied Solid State Science,* R. Wolfe, ed. (Academic, New York, 1972), Vol. 3.
7. J. W. Goodman, *Introduction to Fourier Optics* (McGraw-Hill, New York, 1968).
8. A. Korpel, "Two-dimensional plane wave theory of strong acousto-optic interaction in isotropic media," J. Opt. Soc. Am. **69,** 678–683 (1979).
9. R. Pieper and A. Korpel, "Comparison of phased-array Bragg cells operating in the second order," Appl. Opt. **23,** 2921–2934 (1984).
10. N. Ahmed and T. Natarajan, *Discrete-Time Signals and Systems* (Prentice-Hall, Reston, Va., 1983).